Results in Engineering 20 (2023) 101460

Contents lists available at ScienceDirect

Results in Engineering

journal homepage: www.sciencedirect.com/journal/results-in-engineering

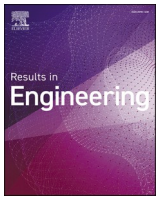

Investigation on swelling behavior of sodium alginate/black titania nanocomposite hydrogels and effect of synthesis conditions on water uptake

K.V. Satheesh Kumar [a], M. Bindu [b], Shwetha Suresh [b], A. Anil [c], S. Sujoy [c], A. Mohanan [d,**], P. Periyat [b,*]

[a] Post Graduate & Research Department of Chemistry, Govt. College, Kasaragod, Kerala, India
[b] Department of Environmental Studies, Kannur University, Kannur, Kerala, India
[c] Department of Materials Engineering, Indian Institute of Science, Bangalore, Karnataka, India
[d] Department of Chemistry, Nehru Arts & Science College, Kanhangad, Kerala, India

ARTICLE INFO

Keywords:
Sodium alginate
Black titania
Cross-linking
Hydrogels
Swelling studies

ABSTRACT

Polymeric nanocomposite hydrogels were developed from a hydrophilic natural polymer, sodium alginate (SA) with black nano crystalline titania (black TiO_2) by using ionic cross linker $CaCl_2$, in view of the possible enhancement in properties of SA towards water treatment application. The optimum conditions for the preparation of films were done by varying the amount of cross-linking agent, cross-linking time and the amount of black nano crystalline TiO_2. The nanocomposite hydrogels were then characterized by X-ray diffraction studies (XRD), fourier transform infrared spectroscopy (FTIR) and thermogravimetric analysis (TGA). The surface morphologies of the nanocomposite have been examined by using scanning electron microscopy (SEM). The swelling studies and its kinetics have been investigated under diverse P^H conditions. Permeability of the gels were assessed in terms of film characteristics and P^H. The results proved that the gels exhibit P^H sensitivity. Based on the results, we have proposed a possible mechanism of water transport through the gels. The developed SA/black TiO_2 nanocomposite hydrogels have been successfully employed for the efficient degradation organic dyes such as methylene blue and malachite green. The experimental results of dye degradation studies have been compared with theoretical models and it has been observed that the dye degradation follows pseudo second order kinetics for both methylene blue and malachite green. By altering the P^H, the nanocomposite hydrogels can be broken and spent TiO_2 can be recovered.

1. Introduction

Hydrogels constitute a category of soft materials, having excellent water retention characteristics, have now been extensively employed in various sectors *viz*; medical, pharmaceutical, agricultural and industrial fields, owing to their intelligent and elastic features [1–6]. Among them, stimuli responsive hydrogels form a distinct group of hydrogels, which undergoes physical or chemical changes with respect to external stimuli *viz*; P^H, temperature, ionic strength, light, electric and magnetic field. Extensive research programs are being going on the fabrication of such hydrogels, exclusively for pharmaceutical and biomedical applications [7–13]. The physical properties of polymers can be improved and new features can be implemented, by adding suitable inorganic nanoparticles within the matrix. It has been reported that, by the judicious selection of the nanoparticles and the polymers, it may possible to achieve multiple stimuli responsive features, owing to the synergy between the nanoparticles and the polymer networks [14–17].

Excellent literature reports are available, based on the reinforcement of a wide range of polymer matrices by a variety of nanoparticles such as ceramic, metal-metal oxide and carbon-based nanoparticles, *via* various synthesis strategies [18–21]. The nanocomposite hydrogels have been observed to exhibit outstanding stability compared to virgin hydrogels, owing to the interaction amongst the nanoparticles and the polymers through van der Waals interactions, hydrogen bonds and electrostatic

* Corresponding author.
** Corresponding author.
E-mail addresses: drmohanan75@gmail.com (A. Mohanan), pperiyat@kannuruniv.ac.in (P. Periyat).

https://doi.org/10.1016/j.rineng.2023.101460
Received 14 April 2023; Received in revised form 25 September 2023; Accepted 25 September 2023
Available online 26 September 2023

interactions. So far, the synthesis strategies adopted for the development of nanocomposite polymer hydrogels include *insitu* polymerisation, *insitu* growth of the nanoparticles and physical mixing [22,23]. *Insitu* polymerisation has been reported to be suitable for the nanoparticles having surface polar groups such as –COOH, NH_2, –OH groups *etc* [24]. The *insitu* growth method of polymerisation may be appropriate for the nanoparticles with intrinsic functions, but hardly surface modified. Physical mixing is the simplest synthesis route to develop polymer nanocomposite hydrogels by merely mixing the partners [25,26]. Preparation of nanocomposite hydrogels, based on natural polymers are highly interesting, owing to its bioactivity and biodegradability [27–29].

Metal oxide nanoparticles can be effectively incorporated into polymeric matrices for waste water treatment with high efficiency. By doing so, the problems associated with metal oxides such as particle aggregations can be minimised and selectivity, adsorption capacity *etc* can be tuned. Various strategies have been employed to eliminate/reduce pollutants from aquatic environment *via* biosorption, adsorption, chemical precipitation, ion exchange, reverse osmosis *etc*. Among them, adsorption has gained special attention owing to the simple working principle and relatively low cost. The selectivity and sensitivity of adsorbent is very important; low selectivity and sensitivity cause the usage of large amount of adsorbent, leads to problems such as accumulation with a high level of pollutant content which is difficult to regenerate [30–32]. Table 1 shows a comparison of the performance of metal oxide-based nanocomposite hydrogels for the removal of contaminants from waste water.

Table 1
A comparison of performance of metal oxide-based nanocomposite hydrogels for the removal of contaminants from waste water.

No	Metal oxide hydrogel	Pollutant	Experimental conditions	Adsorption capacity (mg/g)	Ref
1	MnO_2-porous polyacrylamide	Cu(II) Pb(II)	Temperature: RT Time: 72 h P^H: 6 and 4	84.76 70.90	[33]
2	MnO_2@reduced graphene oxide hydrogel	Pb(II)	Temperature: RT Time: 12 h P^H: 5	356.37	[34]
3	Chitosan/poly (vinyl alcohol)/ CuO	Pb(II)	Temperature: 323 K Time: 60 min P^H: 5	116.8	[35]
4	Al_2O_3/GO Cellulose	Fluoride	Temperature: 303 K Time: 120 min P^H: 5	5.34	[36]
5	ZnO/Alginate	Methylene blue	Temperature: 323 K Time: 90 min P^H: 7	2.543	[37]
6	ZnO-clay/Alginate	Congo red	Temperature: 303 K Time: 120 min	546.89	[38]
7	ZnO/Chitosan	Reactive black	Temperature: 313 K Time: 360 min P^H: 4	189.44	[39]
8	Sodium alginate poly(acrylic acid) @ZnO	Methylene blue	Temperature: 303 K Time: 40 min P^H: 6	1529.6	[40]
9	ZnO/gum arabic grafted polyacrylamide	Malachite Green	Temperature: RT Time: 60 min P^H: 7	766.52	[41]
10	Xanthan gum grafted poly (acrylic acid-*co*-itaconic acid)/ZnO	Methylene blue	Temperature: RT Time: 70 min	212.8	[42]

Sodium alginate, a naturally occurring polymer, one of the important members of polysaccharide family, has been employed for the removal of metal ions, dyes and emerging contaminants in water [43]. They are characterised by environment friendly nature, greater extent of adsorption capacity, biodegradability and easiness in availability. The structure of alginate is very suitable for the uptake of metal ions *via* ion exchange between the cross-linking cation and the pollutant [44]. Their structure consists of a linear block copolymer of 1,4-linked β-D-mannuronic acid and α-L-guluronic acid [45]. The addition of divalent cations such as Ca^{2+} ions into SA results in gel formation. Even though SA hydrogels are being employed for water purification, the undesirable mechanical properties, thermal stability and hydrophilicity limits their application. The functional properties of alginates may be improved by composite fabrication with a suitable partner [46].

TiO_2 is biocompatible, chemically stable, non-toxic and possesses excellent mechanical properties. Literature reports reveal that the incorporation of TiO_2 nanoparticles into different polysaccharide matrices had a positive impact on the mechanical, thermal and physicochemical properties [47]. The discovery of black titania has triggered worldwide scientific interest. They are characterised by structural modification involving self-doped Ti^{3+}/oxygen vacancy or incorporation of H doping. Because of these modifications, electronic, crystal and surface features have been significantly altered. To utilize the visible-light solar energy to meet environmental and energy crises, black TiO_2 as a photocatalyst is an excellent solution to clean polluted water. Black TiO_2 nanomaterials can absorb the entire portion of sunlight (consists of 5% UV, 43% visible and 52% of infrared radiations) and can be used for industrial waste water treatment [48]. Enhancing the optical absorption characteristics of TiO_2 and change of energy level and band-gap of materials can improve their photocatalytic activities [49]. Photocatalysis is frequently utilized to eliminate the organic pigments in water contaminated with dyes by advanced oxidation process [50]. Organic compounds undergo decomposition by reaction with photoactive material in presence of light to give CO_2 and H_2O as the final product [51]. The main characteristics of advanced oxidation process are the production of oxidant species like hydroxyl radical. They have high oxidation power and a potential of 2.8 V, have a significant responsibility in the destruction of organic compounds [52]. The technique has unique advantages such as low energy consumption, high removal efficiency and limited chemical treatment [53–55]. The development of a nanocomposite photocatalyst with high performance under UV and visible light has attracted considerable attention [56,57].

The present work focuses on the development and characterisation of a nanocomposite hydrogel, by using SA and black nano crystalline TiO_2, cross linked by $CaCl_2$, in view of possible enhancement in properties of SA for water treatment applications, by making use of the adsorption characteristics of SA and photocatalytic activity of black TiO_2. There are no literature reports available on the synthesis of SA/black TiO_2 nanocomposite hydrogels. In view of this, SA/black TiO_2 nanocomposite hydrogels have been prepared and the influence of parameters such as amount of cross linker, cross linking time and the amount of black TiO_2 on the swelling features have been studied. By combining the dynamic swelling results and the films characteristics, possible mechanism of water transport through the developed SA/black TiO_2 nanocomposite hydrogels have been proposed. Dye degradation and release studies have been carried out by using methylene blue and malachite green as model dyes.

2. Experimental

2.1. Materials

Titanium (IV) butoxide (97%, Sigma-Aldrich), isopropanol (AR, Sigma-Aldrich), and manganese acetate tetrahydrate (AR, Merck, India) were used for black TiO_2 synthesis. Sodium alginate (SA), calcium

chloride, potassium hydrogen phthalate, potassium dihydrogen orthophosphate, disodium hydrogen orthophosphate dihydrate and hydrochloric acid were procured from S.D. Fine Chemicals, Mumbai, India for the synthesis of polymer. Doubly distilled water was used in the preparation of the films and for the swelling studies.

2.2. Preparation of black titania

The black TiO_2 is synthesized by using a modified method as reported earlier [58]. In a typical procedure, titanium butoxide (6.8 g) was dissolved completely in isopropanol (purity>99.5%, 100 mL) under room temperature, by using a magnetic stirrer. 5 mL of 0.02 M manganese acetate solution was then added to it for hydrolysis and doping. The reaction mixture was stirred for 30 min at room temperature, followed by microwave irradiation for 5 min at 150 °C at 700 W power by using Anton Paar monowave-300 microwave synthesis reactor. The resulting mixture was then cooled to room temperature. A flow chart of synthesis strategy has been shown as Fig. 1.

2.3. Preparation of SA/black titania hydrogels

Aqueous solutions of sodium alginate (SA, 4% (w/v)) were initially prepared by stirring calculated amount of SA for 3 h at room temperature. In order to prepare sodium alginate (SA)/black TiO_2 nanocomposites, varying amounts of black TiO_2 nanoparticles were added to SA solution, followed by stirring for 4 h to get a homogeneous mixture. 5 mL of this solution was poured on a glass plate and solvent evaporation has been carried out at 60 °C to obtain films of average thickness 0.2 mm. The films were then immersed in the crosslinking medium of $CaCl_2$ solution of varying concentration (Table 2). After a definite time period, the samples were taken out from the solution and washed with distilled water to remove excess $CaCl_2$ solution adhering on the surfaces. The films were then vacuum dried at 40 °C and stored in a desiccator. The P^H, cross linking time and the amount of cross linkers are varied to study the effect on polymerisation and quality of the polymer films. A schematic presentation of synthesis of SA/black TiO_2 system has been shown as Fig. 2 and sample formulations and preparation conditions have been shown as Table 2.

2.3.1. Characterisation of the SA/black TiO_2 nanocomposite films

The black TiO_2 and SA/black titania nanocomposite films were characterised by using XRD, FTIR and thermal analysis. The morphology of the nanocomposites was studied by using SEM. XRD patterns were recorded in the diffraction angle range of 20–80°, by using Rigaku diffractometer. FTIR studies were done by using Jasco FTIR-4100 spectrophotometer and morphology by SEM Hitachi S-4800. Thermal analyses were carried out at a temperature range of 35–400 °C, at a heating rate of 20 °C/min, by using PerkinElmer STA 6000 thermal analyzer.

Fig. 1. Schematic presentation of synthesis of black titania.

Table 2
Sample formulations and preparation conditions of SA/black TiO_2 systems.

Sample Code	SA% (w/v)	TiO_2% (w/v)	$CaCl_2$ (molar)	Time (min)	Gel content (%)
SAT0	4	0	0.1	30	86.1
SAT1	4	0.02	0.1	30	88.5
SAT2	4	0.2	0.1	30	82.2
SAT3	4	2	0.1	30	79.5
SAT4	4	0.2	0.05	30	82.5
SAT5	4	0.2	0.5	30	84.9
SAT6	4	0.2	0.1	10	82.2
SAT7	4	0.2	0.1	60	85.5

2.3.2. Swelling studies

Swelling studies of SA/black TiO_2 nanocomposite gels have been carried out at different P^H *viz;* 1.2, 4, 7 and 9.0. The dried, pre weighed samples were immersed in the chosen medium, at room temperature. The films were then removed from the buffered medium after a definite time interval. The liquid drops that adhering on the film surfaces were wiped by using blotting papers and weight increase has been monitored by means of an electronic balance of accuracy ±0.1 mg (Shimadzu ATX224, Japan). The process has been repeated until the films attained an equilibrium swelling. The degree of swelling (S) has been determined by using the equation [11–13]:

$$Swelling(\%) = \frac{Wt - Wo}{Wo} X\ 100 \quad (1)$$

where W_o and W_t, being the weights of the dry and swollen gels, respectively. The percentage (%) equilibrium water content (% EWC) which is defined as the quantity of water that a swollen gel can hold at equilibrium has been evaluated by using the equation:

$$EWC(\%) = \frac{We - Wo}{We} X\ 100 \quad (2)$$

where W_e is the equilibrium weight of the gel. Swelling measurements were triplicated and standard deviations have been incorporated for the figures.

2.3.3. Dye degradation studies

The dye degradation studies were carried out by using SA/black TiO_2 nanocomposite hydrogel granules. Methylene blue and malachite green were used as the model dyes and the measurements were done at λ_{max} 664 nm for methylene blue and 617 nm for malachite green (concentration = 5.85×10^{-5} M). To a definite volume of the dye solution, pre weighed nanocomposite hydrogel granules were added and stirred. After certain intervals of time, a small quantity of sample was taken and optical density was measured to obtain the dye concentration at that time (C). The amount of dye adsorbed per unit mass of adsorbent at equilibrium (q_e) and the amount of dye adsorbed at a time t (q_t) were calculated by using the following equations [38,39]:

$$q_e = \frac{(C_o - C_e) \times V}{W} \quad (3)$$

$$q_t = \frac{(C_o - C_t) \times V}{W} \quad (4)$$

where C_o and C_e are the initial and equilibrium concentrations of the dye solution (mg/L) respectively; V is the volume of the dye solution and W is the weight of the adsorbent. The removal efficiency (%) has been

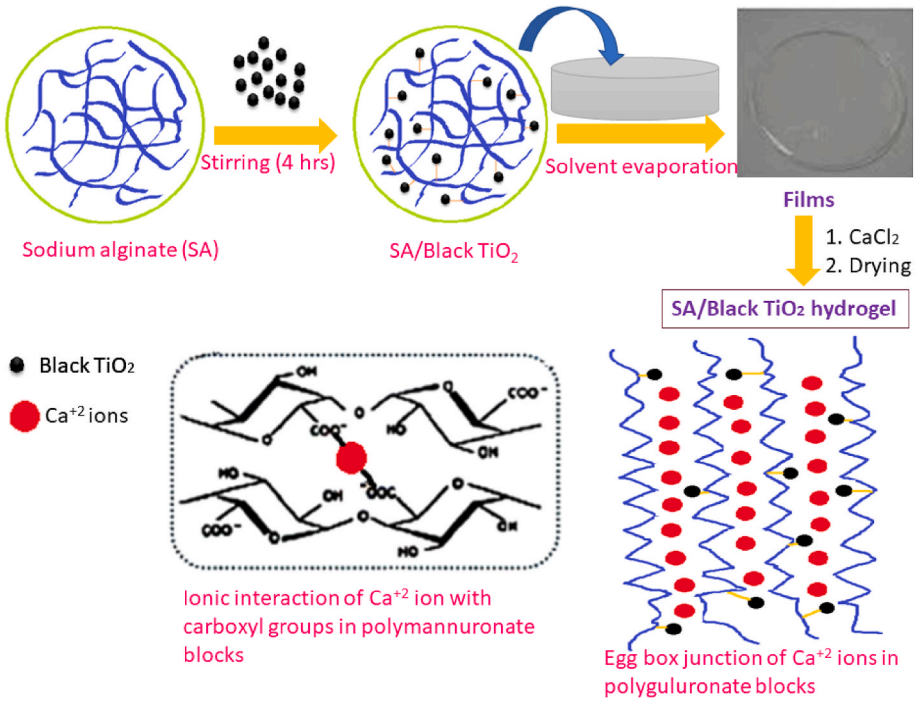

Fig. 2. Schematic presentation of synthesis of SA/black titania nanocomposites (Sample formulations and preparation conditions have been given in Table 2**).**

determined using the equation:

$$R\% = \frac{C_o - C_e}{C_o} \times 100 \quad (5)$$

3. Results and discussion

The XRD patterns of pure SA and SA/black TiO_2 nanocomposites have been shown as Fig. 3. The peaks highlighted in XRD pattern of SA/black TiO_2 nanocomposite (Fig. 3(b)) indicates effective incorporation of black TiO_2 in the SA matrix.

Fig. 4 shows the FTIR spectrum of SA and SA/black TiO_2 nanocomposites. It has been shown that the FTIR spectrum of the nanocomposite film exhibits a broad band at 3400 cm^{-1} owing to the merging

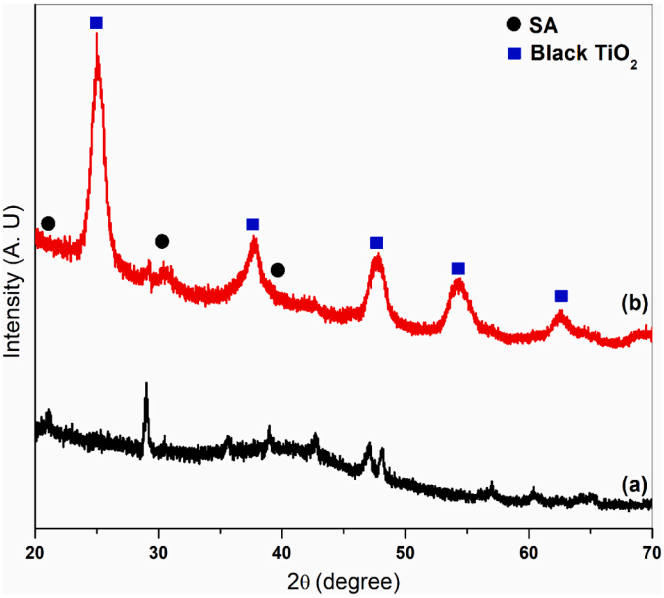

Fig. 3. XRD patterns of (a): SA and (b): SA/black TiO_2 nanocomposites.

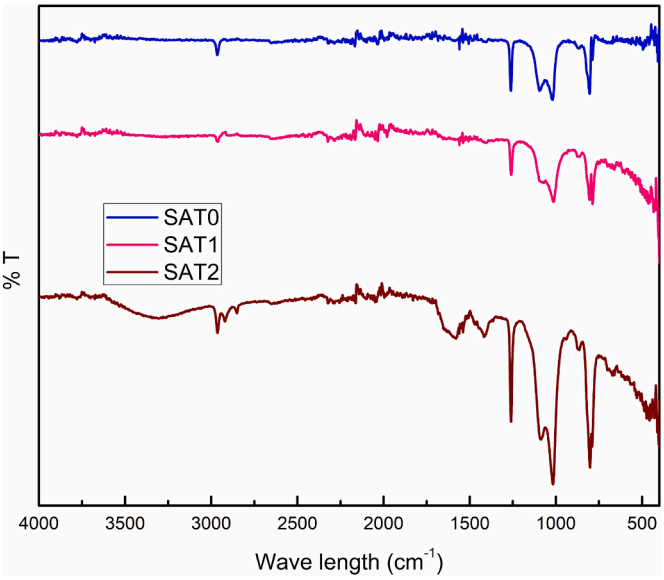

Fig. 4. The FTIR spectra of SA and SA/black TiO_2 nanocomposites.

of stretching vibration of –OH groups in mannuronate and guluronate units of SA and stretching vibrations of Ti–*O*–Ti in TiO_2. As the amount of black TiO_2 increases, the intensity of the peak has been observed to be increased. The C–*O*–C stretching vibrations of SA have been observed at 1030 cm^{-1} and Ti–*O*–Ti stretching mode of vibrations at 1416 cm^{-1} [59].

The thermogravimetric analysis (Fig. 5) showed that the alginate degradation occurs by three steps. During the first stage, at a temperature below 200 °C, the associated water molecules has been removed, owing to the dehydration process and breaking of glycosidic linkages. Second stage of degradation occurs at a temperature range of 200–280 °C, in which alginate skeleton undergoes fracturing. When the temperature further increases, the carboxylate groups undergo

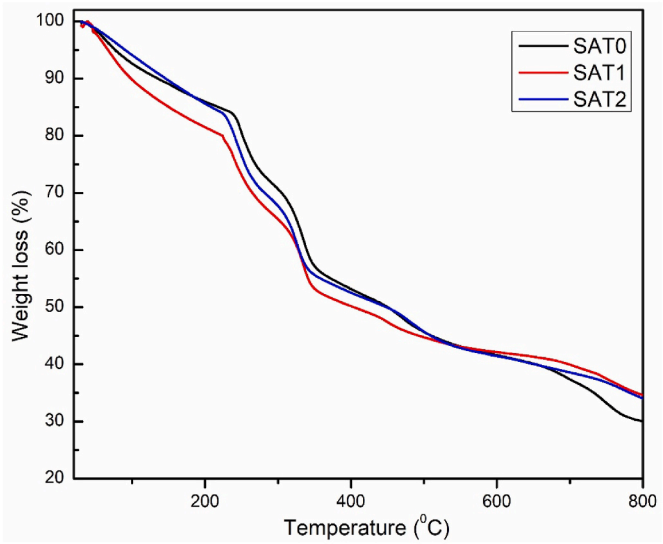

Fig. 5. The TGA curves of pure SA and SA/black TiO_2 nanocomposites.

degradation and releases CO_2. The complete decomposition of alginate occurs at 265 °C. The decomposition temperature of the alginate has been increased upon the incorporation of TiO_2 nanoparticles in the matrix (280 °C).

Fig. 6 shows SEM images of pure SA and SA/black TiO_2 systems (Magnification: 2500×). SEM image of both the SA and black TiO_2 filled SA are clearly distinguishable. Neat SA samples exhibit smooth and homogeneous surfaces, whereas dispersed black TiO_2 nanoparticles can be easily identified in other images (Average particle size is 18 nm). A relatively uniform distribution of nanoparticles are seen in the SEM images. At higher black TiO_2 loading, slight particle agglomeration is visible.

3.1. Swelling studies

Figs. 7–10 show the % swelling of the nanocomposite hydrogels at P^H 7. The swelling features are greatly influenced by the composition of the polymer network, extent of crosslinking and degree of ionization of various functional groups on the polymers. It has been observed that, initially the water absorption by the gel is very high and as the time progress, rate becomes slow down and attains an equilibrium value. From the figures it has been shown that both the initial swelling rate and

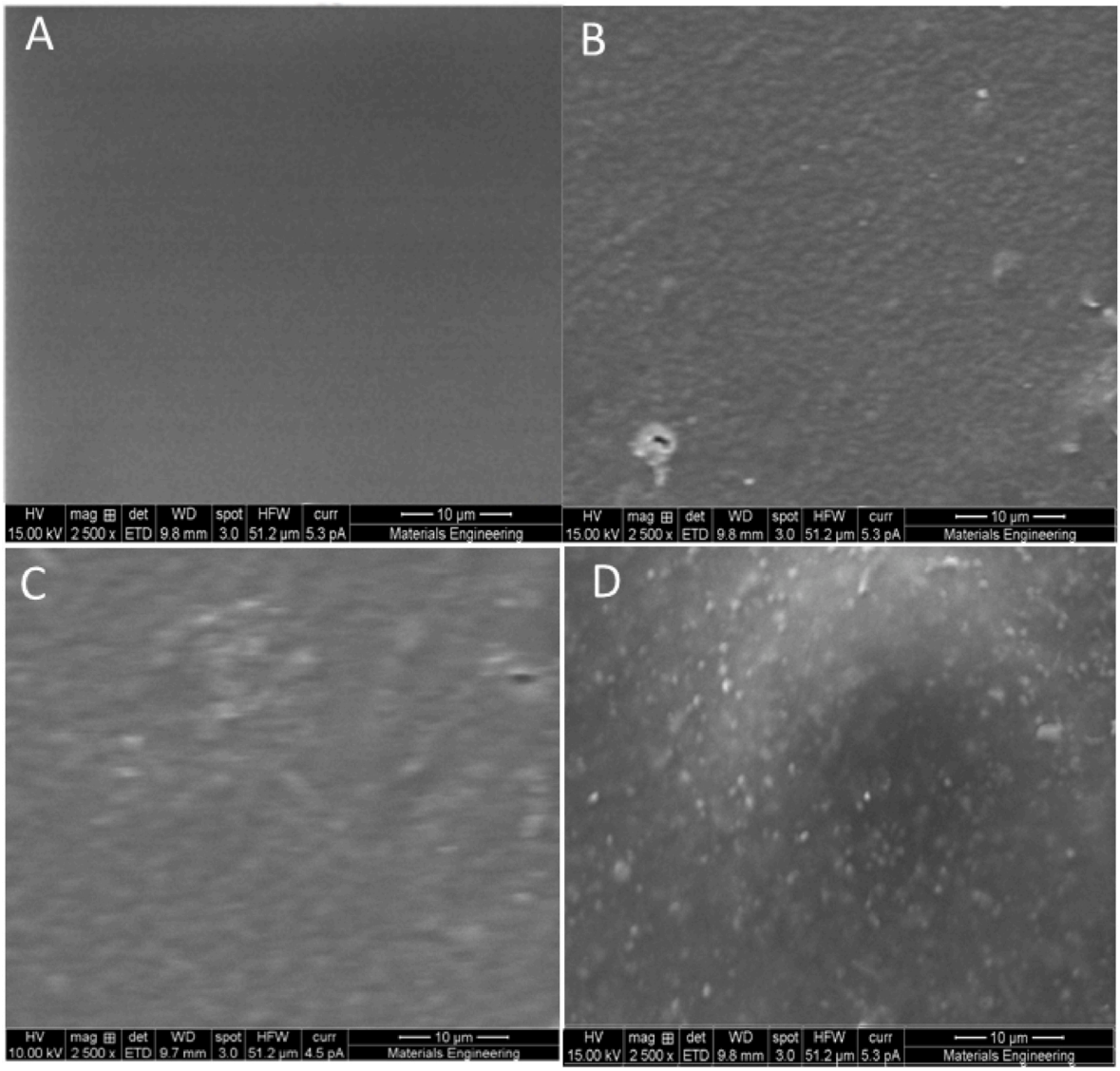

Fig. 6. SEM images of SA and SA/black titania (A: SAT0; B: SAT1, C: SAT2; D: SAT3).

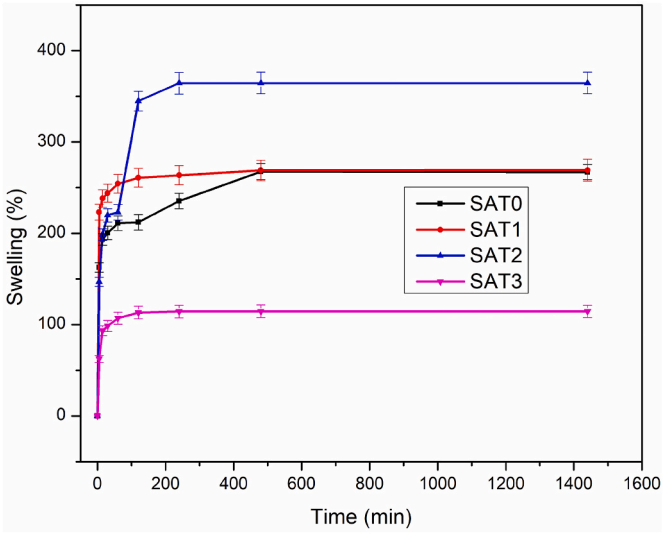

Fig. 7. Swelling (%) *Vs* black TiO_2 content.

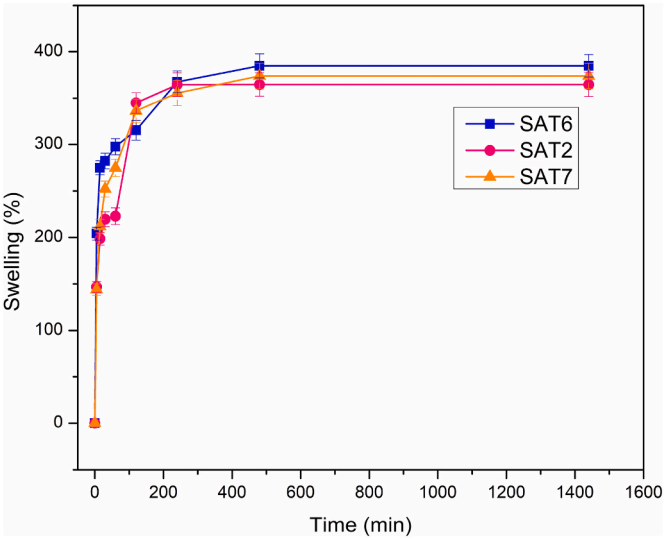

Fig. 9. Swelling % *Vs* crosslinking time.

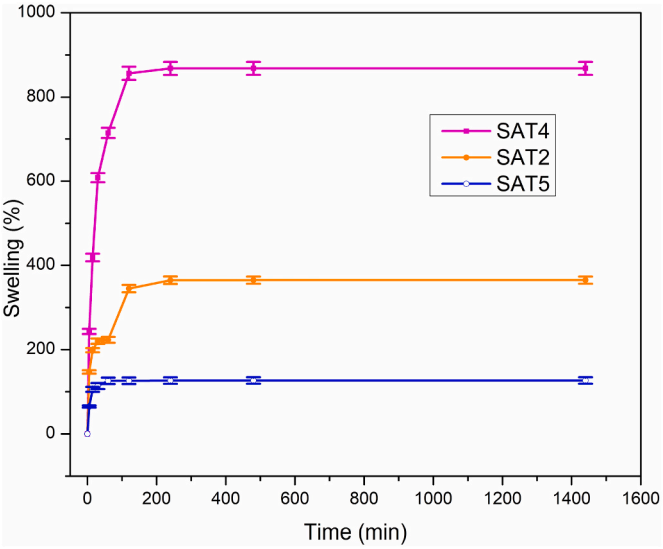

Fig. 8. Swelling (%) *Vs* concentration of the crosslinking agent.

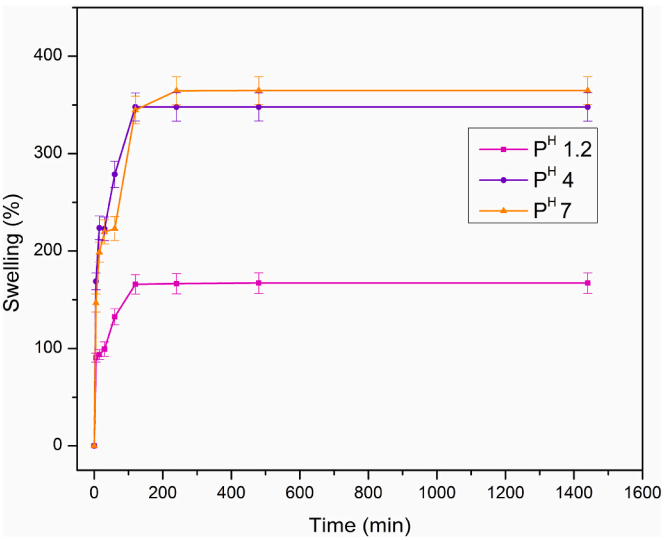

Fig. 10. Swelling % *Vs* P.^{H}.

equilibrium swelling of the gels are influenced by the polymer network.

3.1.1. *Effect of nano composition on the swelling behavior*

To study the influence of black TiO_2 on the swelling features, the composition of black TiO_2 has been varied from 0 to 2 g. The % swelling (S %) increases from 242 to 365 and then decreases to 114, with an increase in the amount of black TiO_2, as indicated by Fig. 7. The maximum swelling has been observed with 0.2 g of black TiO_2. The voids within the polymer matrix have strong influence on the diffusion of solvent molecules through it [60–63].

Nanoparticles may occupy the voids between the polymer chains; there is an increase in free volume to hold more water molecules and hence initially the swelling rate increases. The initial increase may also be due to the wetting property of TiO_2 [64]. As the black TiO_2 loading increases, the voids have been occupied by it, leading to a reduction in % swelling.

3.1.2. *Influence of cross-linker on the swelling characteristics*

As the concentration of the crosslinker $CaCl_2$ and the time of exposure of the nanocomposite gel in the crosslinking medium increases, the number of crosslinks between the polymer networks have been observed to be increasing. From Fig. 8, it is clearly understood that the films cross linked with 0.05 M $CaCl_2$ (SAT4) exhibited an equilibrium swelling ratio of 867, however those crosslinked with 0.1 M (SAT2) and 0.5 M (SAT5) $CaCl_2$ displayed a value of 364 and 127 respectively. To investigate the time period of exposure of the nanocomposite gels to the cross-linking medium on the swelling behaviour, the gels have been cross linked with 0.1 M $CaCl_2$ solutions for 10, 30 and 60 min (SAT6, SAT2 and SAT7). It has been shown that the time of exposure to the crosslinking solution has not much influence on the % swelling (Fig. 9).

3.1.3. *Influence of P^H on the swelling characteristics*

To investigate the influence of P^H on the swelling features, the studies have been carried out at different P^H 1.2, 4.0 and 9.0, besides P^H 7.0. It has been observed that the nanocomposite gels undergo disintegration at P^H 9 and hence no swelling data are available. The swelling results obtained at different P^H *viz;* 1.2, 4 and 7 have been shown as Fig. 10. Maximum swelling percentage has been attained at P^H 7 and minimum at P^H 1.2. It has also been found that the P^H has significant influence on the equilibrium water content of the gels. The carboxylic acid groups of alginates undergo dissociation at P^H 4 and 7 compared to

P^H 1.2, owing to which the gels exhibit P^H sensitivity.

P^{Ka} of alginate is 3.2. Carboxylic acid groups of alginates exist in the form of –COOH at very low P^H (1.2) and as -COO^- at higher P^H. The shrinkage at lower P^H is due to the H-bonding between COOH and OH and the polymer networks expand due to the repulsion between ionized carboxylate (-COO^-), leading to an enhanced water uptake at higher P^H = 7.

3.2. Kinetics of swelling

Kinetics of swelling have been evaluated by means of the expression [65]:

$$\frac{ds}{dt} = ks\left(S_{eq} - S\right)^2 \tag{6}$$

Where S_{eq} is the equilibrium swelling and K_s is the rate constant of swelling. Integrating Eq. (3) over the limits, S = 0 at t = 0 and S═S at t = t, takes the form, t/s = A + Bt.

B is the reciprocal of equilibrium swelling and Ais the reciprocal of the initial swelling rate (R_i) and K_s. Swelling rate (t/s) *Vs* time (t) plot for the representative samples have been shown as Figs. 11 and 12.

The R_i and K_s has been obtained from the intercept of the t/s versus t plot and S_{eq} has been obtained from the slopes. The values have been reported in Table 3. Theoretical S_{eq} values calculated from the plots and experimental values are found in close agreement. It has been found that, the both R_i and K_s values, exhibit a direct relation with the black TiO_2 content in the polymer matrix, and the rigidity of the gels have been governed by the degree of cross-linking. To investigate the mechanism of diffusion, the swelling data were fitted into the equation [66]:

$$F = \frac{W_t - W_o}{W_o} = Kt^n \tag{7}$$

'F' being the swelling power of the gel, defined as the quantity of water confined in the film/unit mass, 'K' being the swelling constant, depends upon the network structure and 'n' is the swelling exponent, that describes the mode of transport of solvents through the polymer matrices. Figs. 13–15 show ln F *Vs* ln t plots of the representative nanocomposite gels. The values of n and K, have been evaluated from the slopes and intercepts of the ln F *Vs* ln t plots and the values have been shown in Table 3. The n values have been found in the range of 0.04–0.22, indicate that the water transport through the nanocomposite gels follows an anomalous mechanism. Reinforcement by black TiO_2 provides high restriction for the rearrangement of the sodium alginate chains to respond to the swelling stress, causes delayed swelling. In the case of anomalous transport, both the solvent diffusion and the chain relaxation rates are comparable.

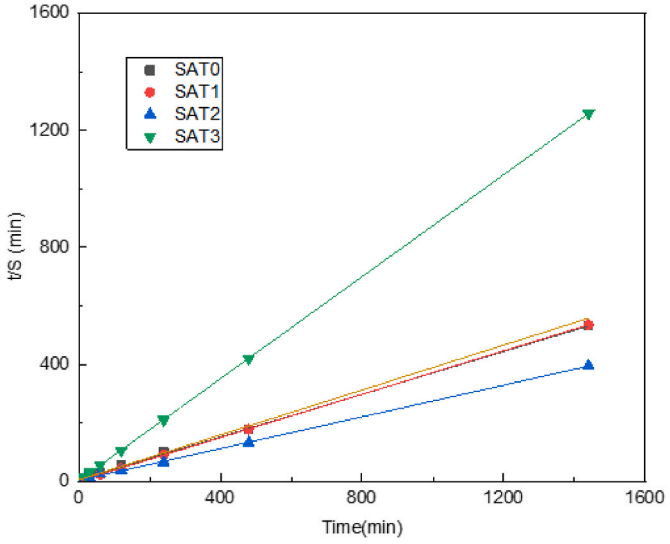

Fig. 11. Swelling rate curves as a function of black TiO_2.

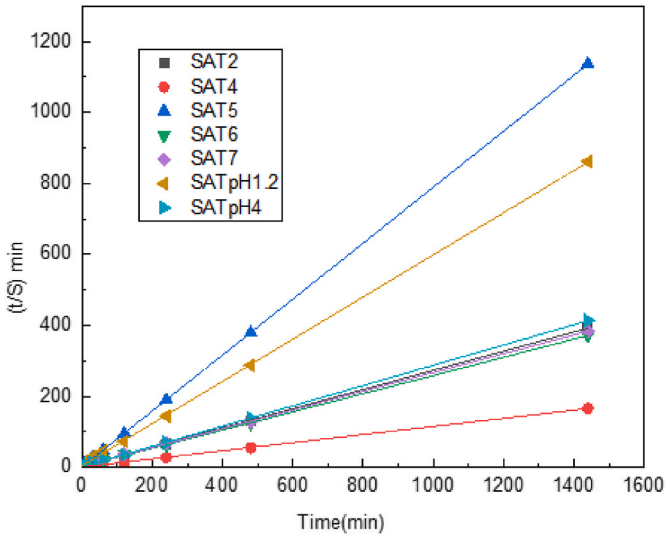

Fig. 12. Swelling rate curves as a function of crosslinking agent and $P.^H$.

3.3. Diffusion studies

Diffusion properties of the SA/TiO_2 nanocomposite gels have been studied by employing the relation [67]:

$$\frac{W_t}{W_\infty} = \frac{4}{r}\sqrt{\frac{Dt}{\pi}} \tag{8}$$

Where 'D' is the diffusion coefficient and 'r' being the radius of the gel. 'D' has been determined from W_t/W_α *Vs* $t^{1/2}$ plots as displayed in Figs. 16 and 17, and the values are tabulated (Table 3). As the concentration of the crosslinking agent increases, the diffusion coefficient decreases. On the addition of black TiO_2, D value increases to a maximum and starts to decrease.

3.4. Evaluation of gel content

For calculation of the gel content, the dried gel initial weight is taken. It is then kept in water for 48 h. Again, dried and dried weight is taken to obtain the final weight. Gel content is the ratio of final weight to initial weight. A gel content of above 70% means a stable gel. The gel content of the developed nanocomposite hydrogels gels have been shown in Table 2. It has been found that the gels prepared are stable after swelling for 48 h followed by drying.

3.5. Dye degradation studies

Fig. 18 is the photograph of SA/black TiO_2 nanocomposite hydrogel granules before and after the adsorption of methylene blue dye. It has been observed that as the amount of TiO_2 increases from 0.2% to 2%, the rate of dye degradation increases. The composition SAT3 has highest dye degradation potential *i. e*; 99% of both methylene blue (by 180 min) and malachite green (by 360 min) were degraded by SAT3 sample.

Three kinetic models *viz;* pseudo first order, pseudo second order and intraparticle diffusion models were used to analyze the kinetics and mechanism of adsorption.

The pseudo first order kinetic model in its linear form can be represented by the equation:

$$\log(q_e - q_t) = \log q_e - \frac{K_1}{2.303}t \tag{9}$$

The terms q_e and q_t refer to the amount of dye adsorbed at

Table 3
Swelling parameters.

Swelling parameters	SAT0	SAT1	SAT2 PH 7	SAT3	SAT4	SAT5	SAT6	SAT7	SAT2 PH 1.2	SAT2 PH 4
Swelling (S%)	271	269	364	114	867	127	384	379	167	348
Eq. water content (EWC%)	73	73	78	53	90	60	79	87	63	78
Eq. swelling % (Seq)	275	269	376	115	891.3	127.6	383.1	380	170.9	355.9
Initial swelling rate (Ri)	0.181	1.72	0.26	0.39	6.039	0.442	3.903	0.32	0.178	0.435
Swelling rate constant (Ks)	0.023	0.24	0.02	0.29	0.076	0.271	0.266	0.02	0.061	0.034
Swelling exponent (n)	0.17	0.03	0.17	0.09	0.22	0.04	0.03	0.11	0.14	0.14
Diffusion constant (K_D)10^{-4} (cm^2min^{-1})	7.1	4.2	11.1	3.2	29.02	4.2	8.6	11.1	6.6	10.0
Swelling constant (k)	1.123	2.11	1.07	0.61	1.95	0.664	1.763	1.16	0.643	1.344

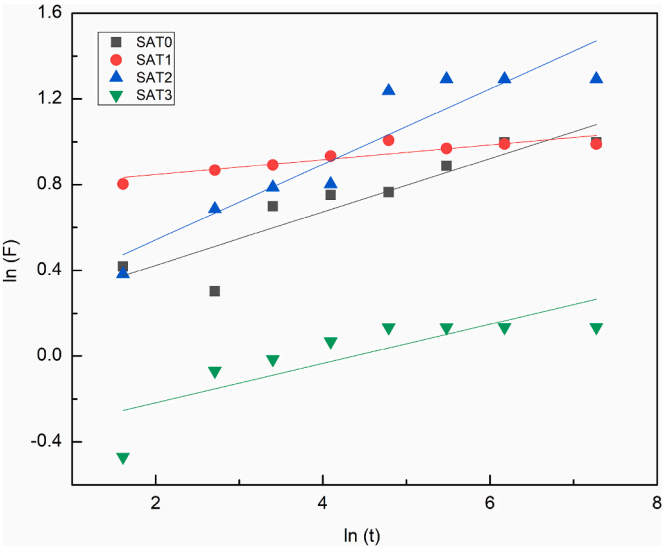

Fig. 13. Swelling power of the gels with concentration of black TiO_2.

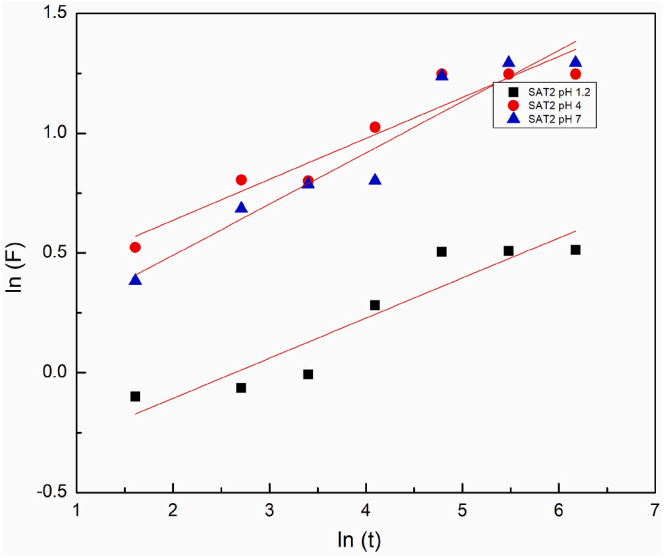

Fig. 14. Swelling power of the gels with concentration of crosslinking agent.

equilibrium (in mg/g) and at time 't' respectively. The pseudo first order adsorption rate constant is shown by the symbol k_1 (min^{-1}). A linear curve with a negative slope will be obtained when log (q_e-q_t) against 't' at various concentrations is plotted. The constants k_1 and q_e can be determined by the curve's slope and intercept, respectively.

The pseudo second order kinetic model can be expressed by the following relation:

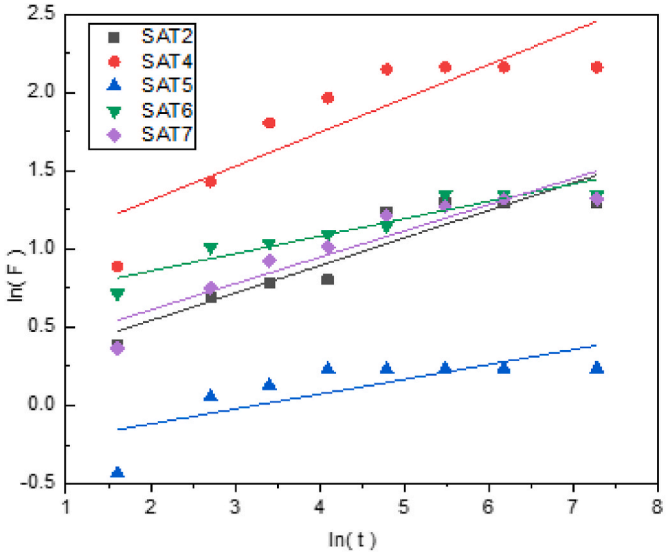

Fig. 15. Swelling power of the gels with P.^{H}.

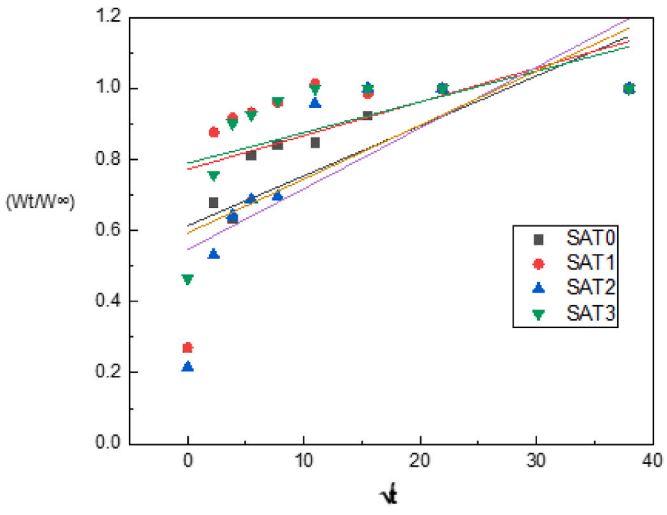

Fig. 16. Diffusion properties as a function of SA content and black TiO_2.

$$\frac{t}{q_t} = \frac{1}{k_2 q_e^2} + \frac{t}{q_e} \tag{10}$$

Here, k_2 is the rate constant for pseudo second order reaction in g/mg min^{-1}. q_e and k_2 can be determined from the slope and intercept of linear plot of t/q_t against 't'.

The mathematical form of intraparticle diffusion model can be expressed as:

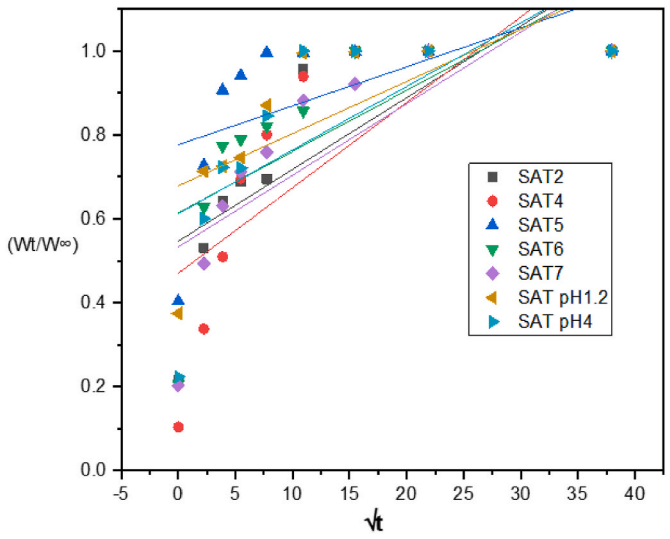

Fig. 17. Diffusion properties as a function of crosslinking agent and P.[H].

$$q_t = k_d\sqrt{t} + C \tag{11}$$

k_d (mg g^{-1} $min^{-1/2}$) and q_t (mg g^{-1}) denote the rate constant for intraparticle diffusion and the amount of dye adsorbed at time 't' respectively, C gives an indication of the boundary layer thickness and is obtained from the slope of q_t versus $t^{1/2}$ plot.

The pseudo first order model, pseudo second order model, and intraparticle models were fitted to account for the experimental values of methylene blue and malachite green adsorption (Fig. 19). The calculated kinetic parameters, including k_1, k_2, and k_{id}, are listed in Table 4. It is clear from Table 4 that the pseudo second order kinetic model provides best match with those of experimental values, and in this instance, the correlation coefficient is more closely related to one. The closeness between the experimental and theoretical values suggests that pseudo second order model govern the adsorption of dyes on the nanocomposite hydrogels.

To understand the favorability of the adsorption and adsorbent-adsorbate interactions, we have evaluated three adsorption isotherm models *viz;* Langmuir, Freundlich and Temkin models. Langmuir adsorption theory describes the formation of monolayer of adsorbed species on homogeneous sites. Mathematically, Langmuir adsorption isotherm can be expressed as:

$$\frac{c_e}{q_e} = \frac{c_e}{q_{max}} + \frac{1}{K_L\, q_{max}} \tag{12}$$

where, c_e, q_e and q_{max} denote the equilibrium concentration of adsorbate, amount of adsorbate adsorbed at equilibrium and maximum monolayer adsorption capacity respectively. K_L being the adsorption equilibrium constant and is related to adsorption rate R_L as:

$$R_L = \frac{1}{1 + K_L C_0} \tag{13}$$

C_o is the initial concentration of the adsorbate (mg/l). The adsorption rate R_L is known as the separation factor, which determines the favorability of adsorption. For a favorable adsorption, the value of R_L is in between 0 and 1. A plot of $c_e/\, q_e$ against c_e is a straight-line having slope $1/q_{max}$ and intercept $\frac{1}{K_L\, q_{max}}$.

According to Freundlich adsorption isotherm, heterogeneous multilayer adsorption takes place and can be expressed as:

$$ln\, q_e = ln\, k_F + \frac{1}{n}\, ln\, c_e \tag{14}$$

where, k_F and n are the isotherm constants. The plot of $ln\, q_e$ *versus* $ln\, c_e$ is a straight line with $\frac{1}{n}$ as the slope and $ln\, k_F$ as the intercept. The value of n determines the favorability of adsorption, if n is in between 1 and 10, the adsorption is favorable and if it is lower than 1 the adsorption is unfavorable.

The Temkin model explains that the heat of molecular adsorption decreases linearly with increasing adsorbent surface coverage. The Temkin isotherm is mathematically expressed as:

$$q_e = BlnA_T + BlnC_e \tag{15}$$

$$B = \frac{RT}{B_T} \tag{16}$$

The constant B is associated with heat of adsorption.

$$A_T = \frac{RTlnk_T}{B_T} \tag{17}$$

k_T is the equilibrium binding constant (L/mol), corresponding to maximum binding energy. If $B > 0$, the process is exothermic and if $B < 0$, it is endothermic. $ln\, c_e$ *versus* q_e plot gives the value of B as the slope and A_T as the intercept.

We have fitted the equilibrium adsorption data for the adsorption of

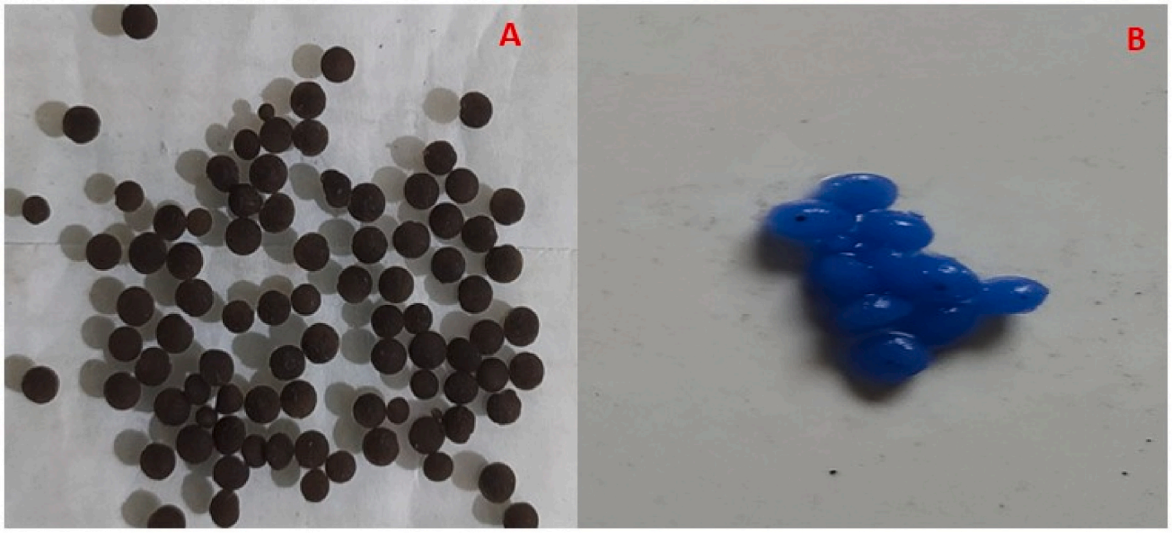

Fig. 18. SA/black TiO_2 nanocomposite hydrogel granules (A): Before the adsorption of methylene blue (B): After the adsorption of methylene blue.

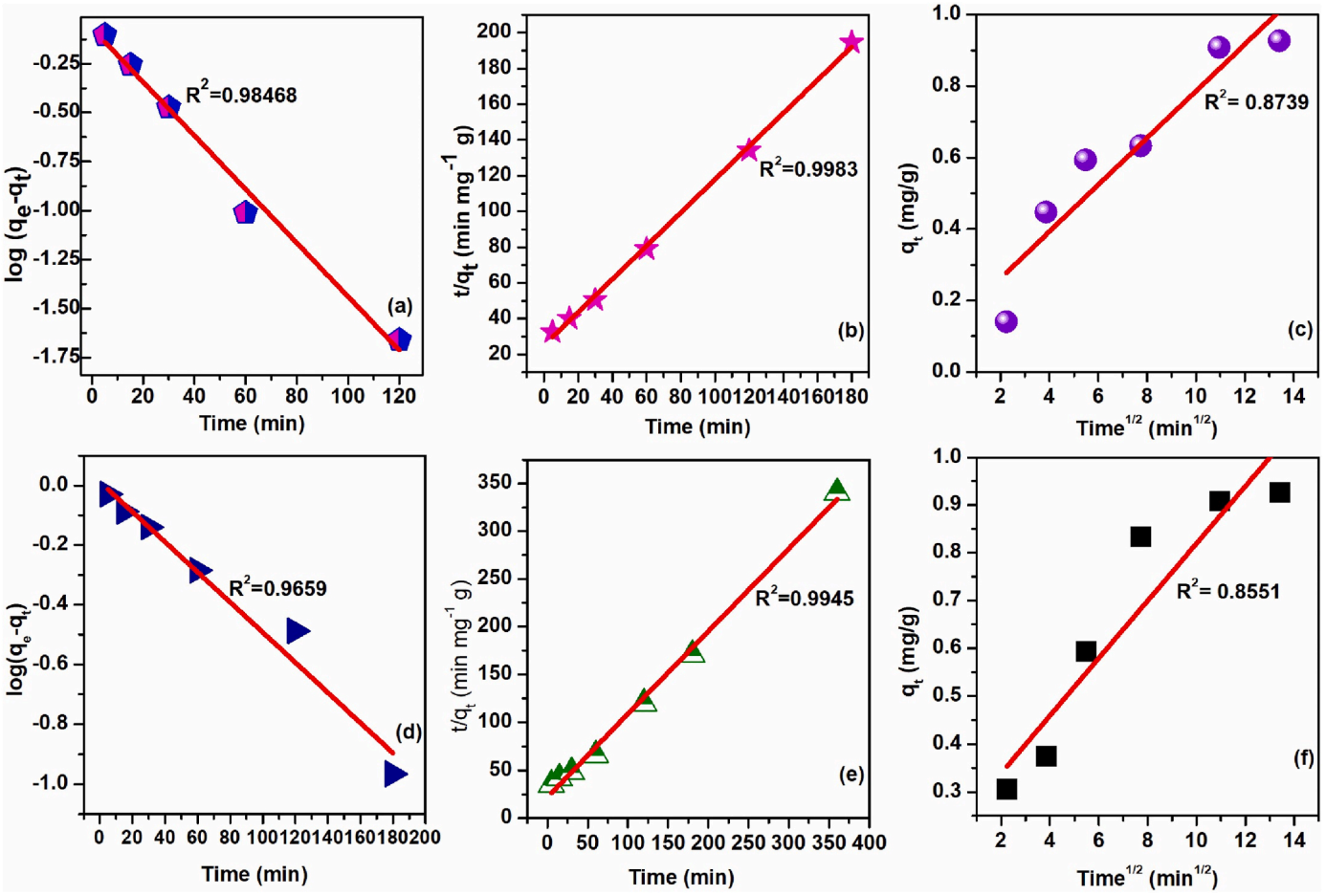

Fig. 19. (a) pseudo first order model for methylene blue dye degradation (b) pseudo second order model for methylene blue dye degradation (c) intraparticle diffusion model for methylene blue dye degradation (d) pseudo first order model for malachite green degradation (e) pseudo second order model for malachite green degradation (f) intraparticle diffusion model for malachite green degradation.

Table 4
Kinetic parameters of the dye adsorption.

No	Dye	Experimental q_e	Pseudo first order model	Pseudo second order model	Intraparticle diffusion model
1	Methylene blue	0.93 mg/g	k_1 = 0.0137 (min^{-1}) R^2 = 0.9846 q_e = 0.0696 mg/g	k_2 = 25.06 (g mg^{-1} min^{-1}) R^2 = 0.9986 q_e = 0.9278 mg/g	k_{id} = 0.0654 (g mg^{-1} $min^{-1/2}$) R^2 = 0.8739 q_e = 0.1313 mg/g
2	Malachite green	1.05 mg/g	k_1 = 0.0050 (min^{-1}) R^2 = 0.9659 q_e = 0.0126 mg/g	k_2 = 22.22 (g mg^{-1} min^{-1}) R^2 = 0.9945 q_e = 0.865 mg/g	k_{id} = 0.0601 (g mg^{-1} $min^{-1/2}$) R^2 = 0.8551 q_e = 0.2188 mg/g

a representative dye malachite green, into these three isotherm models and the resulting linear plots are shown in Fig. 20. Using the linear regression method, the values of correlation coefficients (R^2) and isotherm constants were determined. With high correlation coefficient (R^2 = 0.9974), the Langmuir model provide a better fit for the adsorption of dye. The q_{max} and R_L values were calculated to be 1.06 mg/g and 0.0075 respectively. Since the value of R_L is in between 0 and 1, the adsorption is favorable.

Dye release studies have been carried out at P^H 4, 7 and 9. At P^H 4 and 7, the release was almost same. But maximum release was limited to 35% indicating photo reduction of the dye. At higher P^H, the dye encapsulated hydrogel granules were broken, and the spent TiO_2 can be recovered. Relative concentration versus time plot of a representative sample at various P^H has been shown as Fig. 21.

Competitive degradation of dyes was also tried using a mixture of methylene blue and malachite green. The rate constant is slightly higher in the case of methylene blue (25.69 g mg^{-1} min^{-1}) than malachite green (20.88 g mg^{-1} min^{-1}). Corresponding C/C_0 versus time plot has been depicted as Fig. 22.

4. Conclusions

In recent years, many studies have been carried on the use of biopolymers as adsorbents for water treatment applications, owing to their simple synthesis strategy, biodegradability, environmental friendliness and low cost. These materials can be tuned for specific pollutants removal. Since SA structure possess many anionic groups (hydroxyl and carboxylate functional groups), it can be employed for the removal of cationic impurities from polluted water. However, weak mechanical properties, hydrophilicity and thermal stability restricts their application. In view of this, black TiO_2 nanoparticles have been incorporated into the SA matrix for the improvement in functional properties of SA.

SA/black TiO_2 nanocomposite hydrogel films were developed by

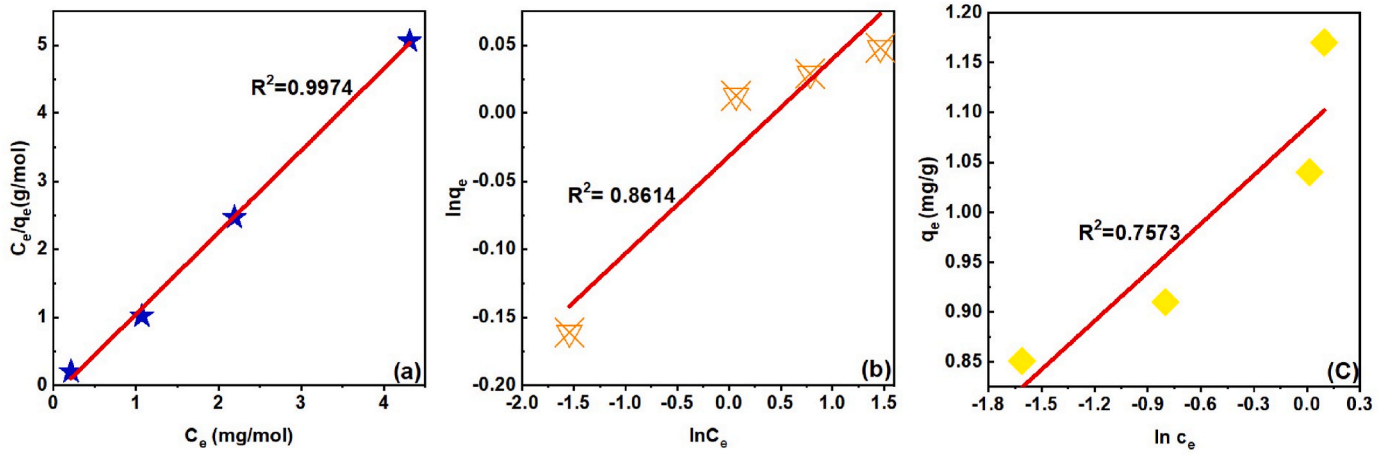

Fig. 20. Adsorption isotherm plots of malachite green; (a) Langmuir (b) Freundlich (c) Temkin model.

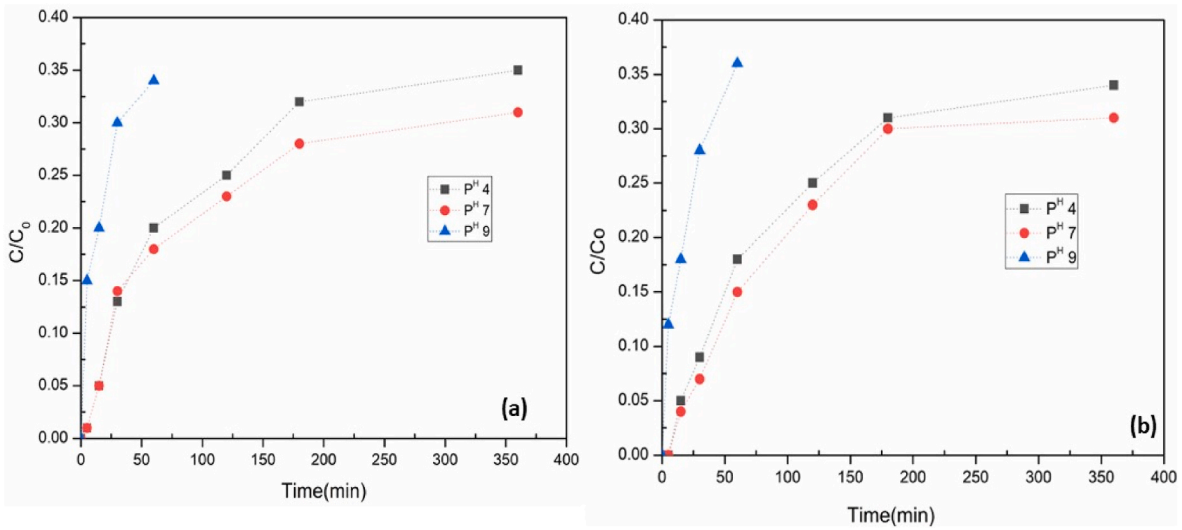

Fig. 21. Dye release at various P^H (a): methylene blue (b): malachite green.

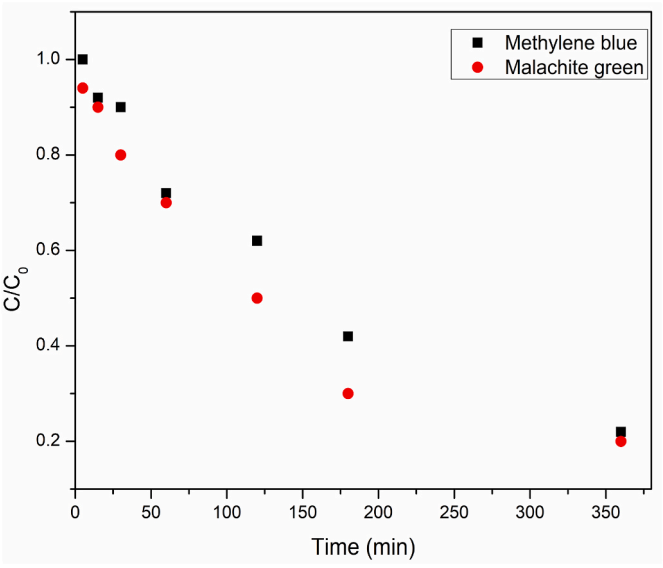

Fig. 22. C/C_0 versus time plot of competitive dye degradation.

using $CaCl_2$ as crosslinking agent. The polymeric nanocomposite films developed were characterized by X-ray diffraction studies, FTIR analysis and thermal studies. X-ray diffraction studies reveal that with an increase in black TiO_2 loading, the crystallinity of the system gets decreased. Black TiO_2 incorporation onto SA enhances the thermal stability. Morphology evaluation by SEM confirms the homogeneity of dispersion of black titania in alginate matrix. Swelling behavior has been investigated with respect to nano compositions, behaviour of cross-linking agent and P^H. Swelling studies showed that they have P^H responsive features and transport of solvents follow anomalous diffusion.

SA/black TiO_2 nanocomposite hydrogels have been employed for the degradation of model dyes *viz;* methylene blue and malachite green. 99% of both methylene blue and malachite green were degraded by the developed SA/black TiO_2 nanocomposite hydrogels. The main attractive feature of the system is its P^H sensitive nature, and can be broken and recovered by altering the P^H.

Declaration of competing interest

The authors declare no conflicts of interest.

Data availability

No data was used for the research described in the article.

Acknowledgements

Authors are thankful to Sheethu K for the data measurements of the samples. Dr. Bindu M. is grateful to KSCSTE for her Back to Lab Post-Doctoral Fellowship (KSCSTE/261/2021 BLP, Council (P) Order No: 161/2021/KSCSTE; dated 13-03-2021).

References

[1] N.A. Peppas, A.R. Khare, Preparation, structure and diffusional behavior of hydrogels in controlled release, Adv. Drug Deliv. Rev. 11 (1993) 1–35, https://doi.org/10.1016/0169-409X(93)90025-Y.

[2] A. Mohanan, B. Vishalakshi, R.N. Charyulu, N.M. Harish, S. Ganesh, Sustained release of metoprolol tartarate from radiation-grafted pH-Responsive Hydrogels, Int. J. Polym. Mater. 58 (2009) 32–48, https://doi.org/10.1080/00914030802461899.

[3] J.E. Tasque, P.A. Raffo, L.A. Sanz, M.R. Sanz, I.N. Vega, N.B.D. Accorso, A new organosilylated hydrogel as loss control materials: synthesis, characterization, and evaluation, Results Eng 17 (2023), 100804, https://doi.org/10.1016/j.rineng.2022.100804.

[4] M.H. Rownok, M. Sabrin, M. Sultana, Ashaduzzaman, S.B. Soumma, Z.R. Saha, Md S. Rahman, A.S.M. Nur, Fabrication of charcoal-nickel (II)-poly(acrylic acid) nanocomposite hydrogels for photodegradation of rhodamine B under direct sunlight irradiation, Results Eng 16 (2022), 100695, https://doi.org/10.1016/j.rineng.2022.100695.

[5] A. Mohanan, B. Vishalakshi, R.N. Charyulu, N.M. Harish, S. Ganesh, Sustained release of Atorvastatin from radiation-synthesized stimuli-responsive hydrogels, Int. J. Polym. Mater. 62 (2013) 5–9, https://doi.org/10.1080/00914037.2011.641636.

[6] C.S. Satish, K. P Satish, H.G. Shivakumar, Hydrogels as controlled drug delivery systems: synthesis, crosslinking, water and drug transport mechanism, Indian J. Pharmaceut. Sci. 68 (2006) 133–140, https://doi.org/10.4103/0250-474X.25706.

[7] Z.H. Cao, Y. Jin, B. Zhang, Q. Miao, C.H. Ma, A novel temperature and p^H responsive polymer-biomolecule conjugate composed of casein and Poly(N-Isopropylacrylamide), Iran. Polym. J. (Engl. Ed.) 19 (2010) 689–698.

[8] M. Zhao, Z. Tang, X. Zhang, Z. Li, H. Xiao, M. Zhang, K. Liu, Y. Ni, L. Huang, L. Chen, H. Wu, A self-healing, stretchable, and conductive poly(N-vinylpyrrolidone)/gallic acid composite hydrogel formed via hydrogen bonding for wearable electronic sensors, Compos. Sci. Technol. 29 (2020), 108294, https://doi.org/10.1016/j.compscitech.2020.108294.

[9] Z. Zhou, C. Qian, W. Yuan, Self-healing, anti-freezing, adhesive and remoldable hydrogel sensor with ion-liquid metal dual conductivity for biomimetic skin, Compos. Sci. Technol. 203 (2021) 108608–108617, https://doi.org/10.1016/j.compscitech.2020.108608.

[10] X. Huang, T.L. Lowe, Biodegradable thermoresponsive hydrogels for aqueous encapsulation and controlled release of hydrophilic model drugs, Biomacromolecules 6 (2005) 2131–2139, https://doi.org/10.1021/bm050116t.

[11] F. Martellinia, L.H.I. Meia, J.L. Balino, M. Carenzad, Swelling and water transport in temperature sensitive hydrogels based on 2-methoxyethylacrylate, Radiat. Phys. Chem. 63 (2002) 29–33.

[12] S.J. Kim, K.J. Lee, S.I. Kim, Thermo-sensitive swelling behavior of poly(2-ethyl-2-oxazoline)/poly (vinyl alcohol) interpenetrating polymer network hydrogels, J. Macromol. Sci., Pure Appl. Chem. 41 (2004) 267–274, https://doi.org/10.1081/MA-120028206.

[13] A. Mohanan, B. Vishalakshi, Swelling and diffusion characteristics of interpenetrating network films composed of sodium alginate and gelatin: transport of Azure B, Int. J. Polym. Mater. 58 (2009) 561–580, https://doi.org/10.1080/00914030903035469.

[14] C. Li, C. Mu, W. Lin, Novel hemocompatible nanocomposite hydrogels crosslinked with methacrylated gelatin, RSC Adv. 6 (2016) 43663–43671, https://doi.org/10.1039/C6RA04609F.

[15] K. Haraguchi, T. Takehisa, Nanocomposite Hydrogels: a unique organic-inorganic network structure with extraordinary mechanical, optical, and swelling/de-swelling properties, Adv. Mater. 14 (2002) 1120–1124, https://doi.org/10.1002/1521-4095(20020816)14:16<1120::AID-ADMA1120>3.0.CO;2-9.

[16] M. Zhu, Y. Liu, B. Sun, W. Zhang, X. Liu, A novel highly resilient nanocomposite hydrogel with low hysteresis and ultrahigh Elongation, Macromol, Rapid Commun 27 (2006) 1023–1028, https://doi.org/10.1002/marc.200600159.

[17] K. Haraguchi, Nanocomposite hydrogels, Curr. Opin. Solid State Mater. Sci. 11 (2007) 47–54, https://doi.org/10.1016/j.cossms.2008.05.001.

[18] M. Liu, Y. Ishida, Y. Ebina, T. Sasaki, T. Hikima, M. Takata, An anisotropic hydrogel with electrostatic repulsion between cofacially aligned nanosheets, Nature 517 (2015) 68–72, https://doi.org/10.1038/nature14060.

[19] X. Xu, Z. Huang, Z. Huang, X. Zhang, S. He, Injectable, NIR/pH-responsive nanocomposite hydrogel as long-acting implant for chemo photothermal synergistic cancer therapy, ACS Appl. Mater. Interfaces 9 (2017) 20361–20375, https://doi.org/10.1021/acsami.7b02307.

[20] W. Wang, Y. Zhang, W. Liu, Bioinspired fabrication of high strength hydrogels from non-covalent interactions, Prog. Polym. Sci. 71 (2017) 1–25, https://doi.org/10.1016/j.progpolymsci.2017.04.001.

[21] A.O. Moughton, M.A. Hillmyer, T.P. Lodge, Multicompartment block polymer micelles, Macromolecules 45 (2012) 2–19, https://doi.org/10.1021/ma201865s.

[22] A. Kumar, M. Jaiswal, Design and in vitro investigation of nanocomposite hydrogel based in situ spray dressing for chronic wounds and synthesis of silver nanoparticles using green chemistry, J. Appl. Polym. Sci. 133 (2016) 43260–43273, https://doi.org/10.1002/app.43260.

[23] M.K. Jaiswal, J.R. Xavier, J.K. Carrow, P. Desai, D. Algae, Mechanically stiff nanocomposite hydrogels at ultralow nanoparticle content, ACS Nano 10 (2016) 246–256, https://doi.org/10.1021/acsnano.5b03918.

[24] L. Guerrini, R.A. Puebla, N.P. Perez, Surface modifications of nanoparticles for Stability in Biological Fluids, Materials 11 (2018) 1154–1181, https://doi.org/10.3390/ma11071154.

[25] T. Zhang, T. Zuo, D. Hu, C. Chang, Dual physically cross-linked nanocomposite hydrogels reinforced by tunicate cellulose nanocrystals with high toughness and good self-recoverability, ACS Appl. Mater. Interfaces 9 (2017) 24230–24237, https://doi.org/10.1021/acsami.7b06219.

[26] L.Z. Zhao, C.H. Zhou, J. Wang, D.S. Tong, W.H. Yu, H. Wang, Recent advances in clay mineral-containing nanocomposite hydrogels, Soft Matter 11 (2015) 9229–9246, https://doi.org/10.1039/C5SM01277E.

[27] X. Qu, A. Wirsen, A.C. Albertsson, Synthesis and characterization of pH-sensitive hydrogels based on chitosan and D, L-lactic acid, J. Appl. Polym. Sci. 74 (1999) 3193–3202, https://doi.org/10.1002/(SICI)10974628(19991220)74:13%3C3193::AIDAPP23%3E3.0.CO;2-V.

[28] K.Y. Lee, D.J. Mooney, Hydrogels for tissue engineering, Chem. Rev. 101 (2001) 1869–1879, https://doi.org/10.1021/cr000108x.

[29] H.J. Choi, R. Yang, M. Kunioka, Synthesis and characterization of p^H-sensitive and biodegradable hydrogels prepared by γ irradiation using microbial poly(γ-glutamic acid) and poly(ε-lysine), J. Appl. Polym. Sci. 58 (1995) 807–814, https://doi.org/10.1002/app.1995.070580414.

[30] Y.A.B. Neolaka, G. Supriyanto, H.S. Kusuma, J. Enviorn. Chem. Eng. 6 (2018) 3436–3443, https://doi.org/10.1016/j.jece.2018.04.053.

[31] Y.A.B. Neolaka, Y. Lawa, J.N. Naat, A.A.P. Riwu, H. Darmokoesoemo, G. Supriyanto, C.I. Holdsworth, A.N. Amenaghawon, H.S. Kusuma, React. Funct. Polym. 147 (2020), 104451, https://doi.org/10.1016/j.reactfunctpolym.2019.104451.

[32] Y.A.B. Neolaka, Y. Lawa, J. Naat, A.A.P. Riwu, Y.E. Lindu, H. Darmokoesoemo, B. A. Widyaningrum, M. Iqbal, H.S. Kusuma, React. Funct. Polym. 166 (2021), 105000, https://doi.org/10.1016/j.reactfunctpolym.2021.105000.

[33] Z. Wu, X. Chen, B. Yuan, M.L. Fu, A facile foaming-polymerization strategy to prepare 3-D MnO_2 modified biochar-based porous hydrogels for efficient removal of Cd(II) and Pb(II), Chemosphere 239 (2020), 124745, https://doi.org/10.1016/j.chemosphere.2019.124745.

[34] T. Zeng, Y. Yu, Z. Li, J. Zuo, Z. Kuai, Y. Jin, Y. Wang, A. Wu, C. Peng, 3D MnO_2 nanotubes @ reduced graphene oxide hydrogel as reusable adsorbent for the removal of heavy metal ions, Mater. Chem. Phys. 231 (2019) 105, https://doi.org/10.1016/j.matchemphys.2019.04.019.

[35] J. Xu, G. Yuvaraja, W. Zhang, Application of chitosan/poly(vinyl alcohol)/CuO (CS/PVA/CuO) beads as an adsorbent material for the removal of Pb(II) from aqueous environment, Colloids Surf., B 149 (2017) 184, https://doi.org/10.1016/j.colsurfb.2016.10.024.

[36] N. Singh, S. Kumari, N. Goyal, S. Khan, Al2O3/GO cellulose based 3D-hydrogel for efficient fluoride removal from water, Environ. Nanotechnol. Monit. Manag. 15 (2021), 100444, https://doi.org/10.1016/j.enmm.2021.100444.

[37] T.M. Tamer, W.M.A. Taleb, G.D. Roston, M.S. Mohyeldin, A.M. Omer, R.E. Khalifa, M. Hafez, Environ. Nanotechnol. Monit. Manag. 10 (2018) 112–121, https://doi.org/10.1016/j.enmm.2018.04.006.

[38] S. Vahidhabanu, D. Karuppasamy, A.I. Adeogun, B.R. Babu, Impregnation of zinc oxide modified clay over alginate beads: a novel material for the effective removal of Congo red from wastewater, RSC Adv. 7 (2017) 5669, https://doi.org/10.1039/C6RA26273B.

[39] S. Cınar, U.H. Kaynar, T. Aydemir, S.C. Kaynar, M. Ayvacıklı, An efficient removal of RB5 from aqueous solution by adsorption onto nano-ZnO/Chitosan composite beads, Int. J. Biol. Macromol. 96 (2017) 459, https://doi.org/10.1016/j.ijbiomac.2016.12.021.

[40] E. Makhado, S. Pandey, K.D. Modibane, M. Kang, M.J. Hato, Sequestration of methylene blue dye using sodium alginate poly(acrylic acid)@ZnO hydrogel nanocomposite: kinetic, Isotherm, and Thermodynamic Investigations, Int. J. Biol. Macromol. 162 (2020) 60–73, https://doi.org/10.1016/j.ijbiomac.2020.06.143.

[41] H. Mittal, P.P. Morajkar, A.A. Alili, S.M. Alhassan, In-Situ synthesis of ZnO nanoparticles using gum Arabic based hydrogels as a self-template for effective malachite green dye adsorption, J. Polym. Environ. 28 (2020) 1637–1653, https://doi.org/10.1007/s10924-020-01713-y.

[42] B.R. Motshabi, K.E. Ramohlola, K.D. Modibane, D. Kumar, M.J. Hato, E. Makhado, Ultrasonic-assisted synthesis of xanthan gum/ZnO hydrogel nanocomposite for the removal of methylene blue from aqueous solution, Mater. Lett. 315 (2022), 131924, https://doi.org/10.1016/j.matlet.2022.131924.

[43] K.Y. Lee, S.H. Yuk, Polymeric protein delivery systems, Prog. Polym. Sci. 32 (2007) 669–697, https://doi.org/10.1016/j.progpolymsci.2007.04.001.

[44] G.T. Grant, E.R. Morris, D.A. Rees, P.J.C. Smith, D. Thom, Biological interactions between polysaccharides and divalent cations-egg-box model, FEBS Lett. 32 (1973) 195–198, https://doi.org/10.1016/0014-5793(73)80770-7.

[45] B.B. Crow, K.D. Nelson, Release of bovine serum albumin from a hydrogel-cored biodegradable polymer fiber, Biopolymers 81 (2006) 419–427, https://doi.org/10.1002/bip.20442.
[46] N.A.S. Abdullah, Z. Mohamad, Z.I. Khan, M. Jusoh, Z.Y. Zakaria, N. Ngadi, Alginate based Sustainable films and composites for Packaging: a Review, Chem. Eng. Trans. 83 (2021) 271–276, https://doi.org/10.3303/CET2183046.
[47] L.M.A. Esparza, Z.V. Mora, J.M.R. Gómez, R.R. Toledo, T.S. Contreras, S. A. Aguirre, E.M. Gonzalez, A.P. Larios, Processes 8 (2020) 1395, https://doi.org/10.3390/pr8111395.
[48] X. Chen, L. Liu, P. Yu, S.S. Mao, Increasing solar absorption for photocatalysis with black Hydrogenated titanium dioxide nanocrystals, Science 331 (2011) 746–750, https://doi.org/10.1126/science.1200448.
[49] J. Chen, Z. Ding, C. Wang, H. Hou, Y. Zhang, C. Wang, G. Zou, X. Ji, Black Anatase titania with Ultrafast sodium-Storage performances Stimulated by oxygen vacancies, ACS Appl. Mater. Interfaces 8 (2016) 9142, https://doi.org/10.1021/acsami.6b01183.
[50] M.A. Mahdi, S.R. Yousefi, L.S. Jasim, M.S. Niasari, Green synthesis of DyBa2Fe3O7.988/DyFeO3 nanocomposites using almond extract with dual eco-friendly applications: photocatalytic and antibacterial activities, Int. J. hydrog. Energy 47 (2022) 14319–14330, https://doi.org/10.1016/j.ijhydene.2022.02.175.
[51] S.R. Yousefi, D. Ghanbari, M.S. Niasari, M. Hassanpour, J. Mater. Sci. Mater. Electron. 27 (2016) 1244–1253, https://doi.org/10.1007/s10854-015-3882-6.
[52] P. Mehdizadeh, M. Jamdar, M.A. Mahdi, W.K. Abdulsahib, L.S. Jasim, S.R. Yousefi, M.S. Niasari, Arab. J. Chem. 16 (2023), 104579, https://doi.org/10.1016/j.arabjc.2023.104579.
[53] S.R. Yousefi, M. Ghanbari, O. Amiri, Z. Marzhoseyni, P. Mehdizadeh, M.H. Oghaz, M.S. Niasari, $Dy_2BaCuO_5/Ba_4DyCu_3O_{9.09}$ S-scheme heterojunction nanocomposite with enhanced photocatalytic and antibacterial activities, J. Am. Ceram. Soc. 104 (2021) 2952–2965, https://doi.org/10.1111/jace.17696.
[54] S.R. Yousefi, H.A. Alshamsi, O. Amiri, M.S. Niasari, Synthesis, characterization and application of Co/Co3O4 nanocomposites as an effective photocatalyst for discoloration of organic dye contaminants in wastewater and antibacterial properties, J. Mol. Liq. 337 (2021), 116405, https://doi.org/10.1016/j.molliq.2021.116405.
[55] S.R. Yousefi, O. Amiri, M.S. Niasari, Control sonochemical parameter to prepare pure Zn0.35Fe2.65O4 nanostructures and study their photocatalytic activity, Ultrason. Sono. 58 (2019), 104619, https://doi.org/10.1016/j.ultsonch.2019.104619.
[56] S.R. Yousefi, A. Sobhani, H.A. Alshamsi, M.S. Niasari, Green sonochemical synthesis of $BaDy_2NiO_5/Dy_2O_3$ and $BaDy_2NiO_5$/NiO nanocomposites in the presence of core almond as a capping agent and their application as photocatalysts for the removal of organic dyes in water, RSC Adv. 11 (2021), 11500, https://doi.org/10.1039/d0ra10288a.
[57] S.R. Yousefi, A. Sobhani, M.S. Niasari, A new nanocomposite superionic system (CdHgI4/HgI2): synthesis, characterization and experimental investigation, Adv. Powder Technol. 28 (2017) 1258–1262, https://doi.org/10.1016/j.apt.2017.02.013.
[58] X. Liu, G. Zhu, X. Wang, X. Yuan, T. Lin, F. Huang, Progress in black titania: a new Material for advanced photocatalysis, Adv. Energy Mater. 6 (2016) 1600452–1600481, https://doi.org/10.1002/aenm.201600452.
[59] V. Vetrivel, K. Rajendran, V. Kalaiselvi, Synthesis and characterization of pure titanium dioxide nanoparticles by sol-gel method, Int. J. Chem. Research. 7 (2014) 1090–1097.
[60] M. Bindu, G. Unnikrishnan, Transport features of nano-hydroxylapatite (n-HA) embedded silicone rubber (SR) systems: influence of SR/n-HA interaction, degree of reinforcement and morphology, Phys. Chem. Chem. Phys. 19 (2017) 25380–25390, https://doi.org/10.1039/C7CP04146B.
[61] J. Abraham, H.J. Maria, S.C. George, N. Kalarikkal, S. Thomas, Transport characteristics of organic solvents through carbon nanotube filled styrene butadiene rubber nanocomposites: the influence of rubber-filler interaction, the degree of reinforcement and morphology, Phys. Chem. Chem. Phys. 17 (2015) 11217–11227, https://doi.org/10.1039/C5CP00719D.
[62] R. Stephen, K. Joseph, Z. Oommen, S. Thomas, Molecular transport of aromatic solvents through microcomposites of natural rubber (NR), carboxylated styrene butadiene rubber (XSBR) and their blends, Compos. Sci. Technol. 67 (2007) 1187–1194, https://doi.org/10.1016/j.compscitech.2006.05.009.
[63] J. George, S.S. Bhagawan, S. Thomas, Effects of environment on the properties of low-density polyethylene composites reinforced with pineapple-leaf fibre, Compos. Sci. Technol. 58 (1998) 1471–1485, https://doi.org/10.1016/S0266-3538(97)00161-9.
[64] C. Zhou, J. Cheng, K. Hou, A. Zhao, P.H. Pi, X. Wen, S. Xu, Superhydrophilic and underwater superoleophobic titania nanowires surface for oil repellency and oil/water separation, Chem. Eng. J. 301 (2016) 301249–301256, https://doi.org/10.1016/j.cej.2016.05.026.
[65] S. Ekici, D. Saraydin, Synthesis, characterization and evaluation of IPN hydrogels for antibiotic release, Drug Deliv. 11 (2004) 381–388, https://doi.org/10.1080/10717540490884804.
[66] Y. Murali, P.S.K. Murthy, B. Sreedhar, K.M. Raju, Swelling and thermal characteristics of pH sensitive crosslinked poly(acrylamide-co-calcium methacrylate) superabsorbent copolymers, J. Appl. Polym. Sci. 102 (2006) 11–12, https://doi.org/10.1002/app.23562.
[67] W.F. Lee, W.H. Chiang, Swelling and drug-release behavior of the poly (AA-co-N-vinyl pyrrolidone)/chitosan interpenetrating polymer network hydrogels, J. Appl. Polym. Sci. 91 (2004) 2135–2142, https://doi.org/10.1002/app.13353.